Meteorology and Atmospheric Physics (2019) 131:897–916
https://doi.org/10.1007/s00703-018-0612-7

ORIGINAL PAPER

Projection of seasonal summer precipitation over Indian sub-continent with a high-resolution AGCM based on the RCP scenarios

Sumin Woo[1] · Gyan Prakash Singh[2] · Jai-Ho Oh[1] · Kyoung-Min Lee[3]

Received: 5 February 2018 / Accepted: 20 May 2018 / Published online: 31 May 2018

Abstract
Seasonal changes in precipitation characteristics over India were projected using a high-resolution (40-km) atmospheric general circulation model (AGCM) during the near- (2010–2039), mid- (2040–2069), and far- (2070–2099) futures. For the model evaluation, we simulated an Atmospheric Model Intercomparison Project-type present-day climate using AGCM with observed sea-surface temperature and sea-ice concentration. Based on this simulation, we have simulated the current climate from 1979 to 2009 and subsequently the future climate projection until 2100 using a CMCC-CM model from Coupled Model Intercomparison Project phase 5 models based on RCP4.5 and RCP8.5 scenarios. Using various observed precipitation data, the validation of the simulated precipitation indicates that the AGCM well-captured the high and low rain belts and also onset and withdrawal of monsoon in the present-day climate simulation. Future projections were performed for the above-mentioned time slices (near-, mid-, and far futures). The model projected an increase in summer precipitation from 7 to 18% under RCP4.5 and from 14 to 18% under RCP8.5 from the mid- to far futures. Projected summer precipitation from different time slices depicts an increase over northwest (NWI) and west-south peninsular India (SPI) and a reduction over northeast and north-central India. The model projected an eastward shift of monsoon trough around 2° longitude and expansion and intensification of Mascarene High and Tibetan High seems to be associated with projected precipitation. The model projected extreme precipitation events show an increase (20–50%) in rainy days over NWI and SPI. While a significant increase of about 20–50% is noticed in heavy rain events over SPI during the far future.

1 Introduction

Climate change can be considered as a fluctuation in atmospheric components over a longer time scale and long-term fluctuations in atmospheric components have a major impact on human activities. In the recent past, heavy rain events caused by climate change have resulted in devastating floods and landslides, causing severe loss of human life and economy of the south Asian countries. The living environment and society are highly sensitive to the duration of extreme events. The agriculture sectors, food, and energy security of India are closely associated with the severity of weather events. Therefore, a proper understanding and advance prediction of the climate change characteristics are important to respond the adoption policies.

The Intergovernmental Panel on Climate Change (IPCC 2007) in the Fourth Assessment report (IPCC AR4) mentioned an increase in surface air temperature (by 0.2 °C/decade) globally and more frequent occurrences of extreme events like heat waves, heavy rain events, etc. Although the possible changes in extreme events induced by global warming were described in IPCC report but the horizontal resolution of the climate models needs more attention. In IPCC AR5 (2013), a large number of climate models are run of the order of more than 100 km in horizontal resolutions, due to the centennial to millennial timescales and non-availability of good computing resources. Although there is a remarkable advancement in climate models during the

Responsible Editor: S. Hong.

✉ Jai-Ho Oh
jhoh@pknu.ac.kr

[1] Department of Environmental and Atmospheric Sciences, Pukyong National University, 45, Yongso-ro, Nam-gu, Busan 48513, South Korea

[2] Department of Geophysics, Institute of Science, Banaras Hindu University, Varanasi 221005, India

[3] CRAY Korea Inc, #317, 27, Seochojungang-ro, Seocho-Gu, Seoul 06601, South Korea

recent few decades, the horizontal resolution of most of the global models is still relatively coarse (above 100 km). This avoids them from reproducing the actual sub-grid scale forcings that have a large impact on the climate at the regional scales. Especially, Indian summer monsoon rainfall (ISMR) which accounts approximately 75–80% of the total yearly rainfall has shown a large interannual variability in the Asian monsoon system. The ISMR is highly affected by complex interactions of various monsoon processes, irregular topography, diverse land surfaces, and surrounding oceans (Rajendran et al. 2013). Therefore, it is hard to get an accurate forecast of seasonal precipitation over India for agriculture, power generation, industry, etc. Rajendran et al. (2013) mentioned that the Global Circulation Models (GCMs) generally failed to capture the detailed features of local climate due to resolution problem. Therefore, they studied the ISMR and extremes weather cases at 20-km high-resolution using an MRI-AGCM for the historical period (1979–2003) and end of century (2075–2099) climates. Although it is possible to study the future climate projection for a partial period, using an ultra-high-resolution model that can represent a better fine-scale structures such as Western Ghats over India (Rajendran and Kitoh 2008). Due to limitations of the computing facility, regional climate models (RCMs) could be used for the study of regional details at a high resolution (Giorgi and Mearns 1999; Hong and Kanamitsu 2014; Lee and Hong 2014). In general, the performances of RCMs are highly related to the performance of the GCMs (Saini et al. 2015), because RCMs use lateral boundary forcings from the GCMs.

Several studies have examined the changes in ISMR and extreme events using different types of the greenhouse emission scenarios. Using the Met Office Hadley Center coupled model (HadCM3), Turner et al. (2007) projected an increase in ISMR in doubled CO_2 experiment. Meehl et al. (2007) found an increase in JJA (June–August) precipitation with the larger inter-models spread in projections over India during 2080–2099 in the Coupled Model Intercomparison Project phase 3 (CMIP3). For extreme events, Turner and Slingo (2009) investigated the change in extreme indices (on 95th and 99th percentile of precipitation) using CMIP3 multi-models and found a similar change as in mean wind field, but with a larger magnitude. Kripalani et al. (2007a, b) extensively studied the IPCC AR4 contributing models simulated data sets, found an enhancement in summer rain over South and East Asia regions at the end of the twenty-first century. Sabade et al. (2011) assessed the CMIP3 models and noted that ten models out of total 25, reasonably well-simulated the annual cycles of ISMR over South Asia. They have found a significant decrease in south westerlies wind fields over South Asia in A1B, A2, and B1 scenarios simulations by ten best performing CMIP3 models, but reported a significant increase in total ISMR. While other researchers (Zhao and Bailey-Kellogg 1998; Ashfaq et al. 2009) have projected a decrease or minor change in ISMR during the same period, Ashrit et al. (2003) have shown that future changes in land–ocean contrast could be stronger and projected an increased ISMR are likely to be related to a northward shift of the Somali jet. Similar results of weak monsoon westerlies over South Asia can be seen in Ueda et al. (2006) using the subset of CMIP3 models, although projected an increased ISMR in the future.

It is well-known facts that the global warming transported more moisture in the lower troposphere and these transported moistures are directly related to the condition of extreme precipitation events (Trenberth et al. 2005). Some of the studies projected a significant change in ISMR especially in or after mid-century climate (Ramanathan et al. 2005; Ramesh and Goswami 2007; Dash et al. 2007). While other researchers have shown that the intraseasonal distribution of ISMR will be more extremes (Goswami et al. 2006; Dash et al. 2009) in the future. Recently, Srivastava et al. (2015, 2016) found an increase in hot days (at the rate of 5.4 days/decade) and a decline in cold days (2.4 days/decade) over India. Based on observed gridded data of IMD, they have also shown an increase in the frequency of heavy rain events of above 100 and 200 mm/day. The above-mentioned studies clearly indicate a large diversity in the model's results. Hence, more careful studies using the high-resolution models are needed for getting better projection over Indian sub-continent.

The present study is, therefore, aimed to investigate the changes in seasonal monsoon characteristics over India from the present-day climate to the future climate (until 2100) continuously using a high-resolution Atmospheric Global Climate Model (AGCM) on the icosahedral–hexagonal grids. After model validation for seasonal mean precipitation, circulations, annual cycle with the various observed data sets, we assess the projected changes in temperature, precipitation, circulations, extreme indices, etc. Descriptions of the high-resolution AGCM (GME) [it has been named GME, because it replaced the operational global model (GM) and the regional model for the central Europe (EM)] and designs of the experiments are introduced in Sect. 2. Section 3 describes the model evaluation. Projected temperature, precipitation, large-scale circulations, extreme indices, etc. are discussed in Sect. 4. Our conclusions are summarized in Sect. 5.

2 Description of GME model, observed data, and simulation details

2.1 GME model

The GME (AGCM) used here is an operational global Numerical Weather Prediction (NWP) model of German Weather services (Majewski et al. 2002). The GME worked on uniform icosahedral–hexagonal grids (brief descriptions about grid shape generation are given in Appendix 1). This method provides two advantages: first, it avoids the pole problem in latitude–longitude grids which is a major drawback of spectral technique. Second, it provides the data structure which is well-suited and enhanced the efficiency of distributed memory parallel computers. The mass flux convection scheme was used for the cumulus parameterization (Tiedtke 1989). For long-term simulation, the mass correction was applied in GME model (Chaudhari 2006). In this study, GME has been run at high resolution ($n_i = 192$, L40) such as 40-km corresponding to T_L511 of ECMWF, where n_i is the number of equal intervals into which each side of the original icosahedral triangles is divided. In n_i 192 (40-km mesh size), the number of grid points are 368,642 and transform grid uses 900×451 grid cells. GME has 40 levels in vertical with a model top at 10 hPa. Detailed descriptions of the GME experiment are summarized in Table 1.

Chaudhari (2006) described the model performance in NWP mode by simulating the severe weather events like typhoons and associated heavy precipitation events over East Asia. In long-term seasonal prediction, model performance was tested by examining the impact of sea-surface temperature and associated atmospheric conditions over South and East Asia monsoons. Recently, using GME, Woo et al. (2018) have projected the teleconnection between South and East Asian summer monsoon systems during twenty-first century and recommended for the study of long-term simulation like future climate change characteristics over Asia region.

Table 1 Detail descriptions of the GME model configuration

Model configuration	
Horizontal resolution	40 km (ni192)
Grid points	900×451
Vertical levels	40 (top at 10 hPa)
Time step	133.33 s
Convection scheme	Tiedtke (1989)
Cloud microphysics	Doms and Schättler (1999)
Radiative transfer of solar and thermal radiation	Ritter and Geleyn (1992)
Vertical turbulent fluxes	Müller (1981)
Sub-grid-scale orographic effects	Lott and Miller 1997
Soil model	Heise and Schrodin (2002)

2.2 Experiment design

With GME, simulations are performed for (a) present-day climate for evaluating model performance and (b) continuously for selecting desired three-time slices in the future for climate change projection. For the model evaluation, we have performed the present-day climate simulation at 40-km horizontal resolution for 30-year periods from 1979 to 2008 (considered as a present-day/current/reference climate). In the present study, we simulated an Atmospheric Model Intercomparison Project (AMIP)-type present-day climate using a GME (40-km) with sea-surface temperature (SST) and sea-ice concentration (SIC) data observed by the National Center for Atmospheric Research (NCAR) following a procedure described by Hurrell et al. (2008). In addition, for the future climate projection, GME was first integrated for the present-day climate from 1979 to 2009 and sequentially future climate simulation from 2010 to 2100 with the future SST and SIC boundary conditions. These boundary data are the projected SST and SIC of the Centro Euro-Mediterraneo sui Cambiamenti Climatici Climate Model (CMCC-CM) of the Coupled Model Intercomparison Project phase 5 (CMIP5) participating models based on the Representative Concentration Pathway (RCP) scenarios by IPCC Fifth Assessment Report (AR5). The CMCC-CM (Scoccimarro et al. 2011) model has a relatively high resolution (0.75°×0.75°) in CMIP5 models. Both monthly observed and projected SST and SIC data are converted into daily data using temporal linear interpolation technique. In addition, we forced the changes in CO_2 concentration and other greenhouse gasses yearly from RCP database (reference: http://www.iiasa.ac.at/ web-apps/tnt/RcpDb) for future climate simulation.

2.3 Observed data

The model performance was evaluated in the present-day climate simulation. Here, monthly precipitation from CPC Merged Analysis of Precipitation (CMAP) data at 2.5° lat/long grid for 30 years (1979–2008) by Xie and Arkin (1997) and the Global Precipitation Climatology Project (GPCP) data on 2.5° lat/long grid for 30 years (1979–2008) by Adler et al. (2003) and Huffman et al. (2009) have been utilized. To analyze the detailed characteristics of precipitation over Indian landmass, the gridded data of India Meteorological Department (IMD) were also studied. Its spatial resolution is 0.5° lat/long grid and it covers only over Indian land points (Rajeevan et al. 2006). For other variables, we have considered the National Center for Environmental Prediction/Department of Energy (NCEP/DOE) Reanalysis II

data (Kanamitsu et al. 2002, hereafter NCEP2) from 1979 to 2008 with the spatial resolutions of 2.5°.

3 Evaluation of present-day climate simulations

3.1 Seasonal precipitation

The GME model is used first time for projecting mean seasonal monsoon characteristics in summer (JJAS) and winter (DJF) over India at 40-km horizontal resolutions in three different time slices in the future during the twenty-first century. Therefore, a proper validation is required to make certain whether GME is able to simulate the present-day monsoon condition before analyzing the future projection. Seasonal precipitation simulated in the present-day climate is validated against the observed precipitation data sets of GPCP (precipitation data available over entire South Asian domain) and IMD (only over land points on $0.5° \times 0.5°$ grids). We have evaluated the long-term climate simulation at a 40-km horizontal resolution over India from 1979 to 2008 (30 years). GME-simulated seasonal precipitation in summer (JJAS) and winter (DJF) is compared to the above-mentioned observed data sets for the period 1979–2008 (Fig. 1). The simulation for the present-day climate has been started from 1979, because observed GPCP precipitation is available from that year only. Here, the present study focuses on surface temperature (at 2 m) and precipitation characteristics. Statistical correlation shows that the model represents the spatial features perfectly well with a very high magnitude of pattern correlation (>0.9) between model and observed (NCEP2) surface air temperature.

The observed climatological summer monsoon (JJAS) precipitation features have found the belts of high precipitation over western Ghats, northeast India and northern Bay of Bengal (BoB), while a low precipitation over northwest India and east coast of India (Fig. 1a). The mean JJAS precipitation simulated by GME (Fig. 1b) is able to reproduce these belts of high and low precipitation reasonably well. For winter (DJF) season, GME well-captured the precipitation over Jammu and Kashmir regions, northeast and southern tips of India mainly over Tamilnadu and Kerala regions. However, model underestimated the

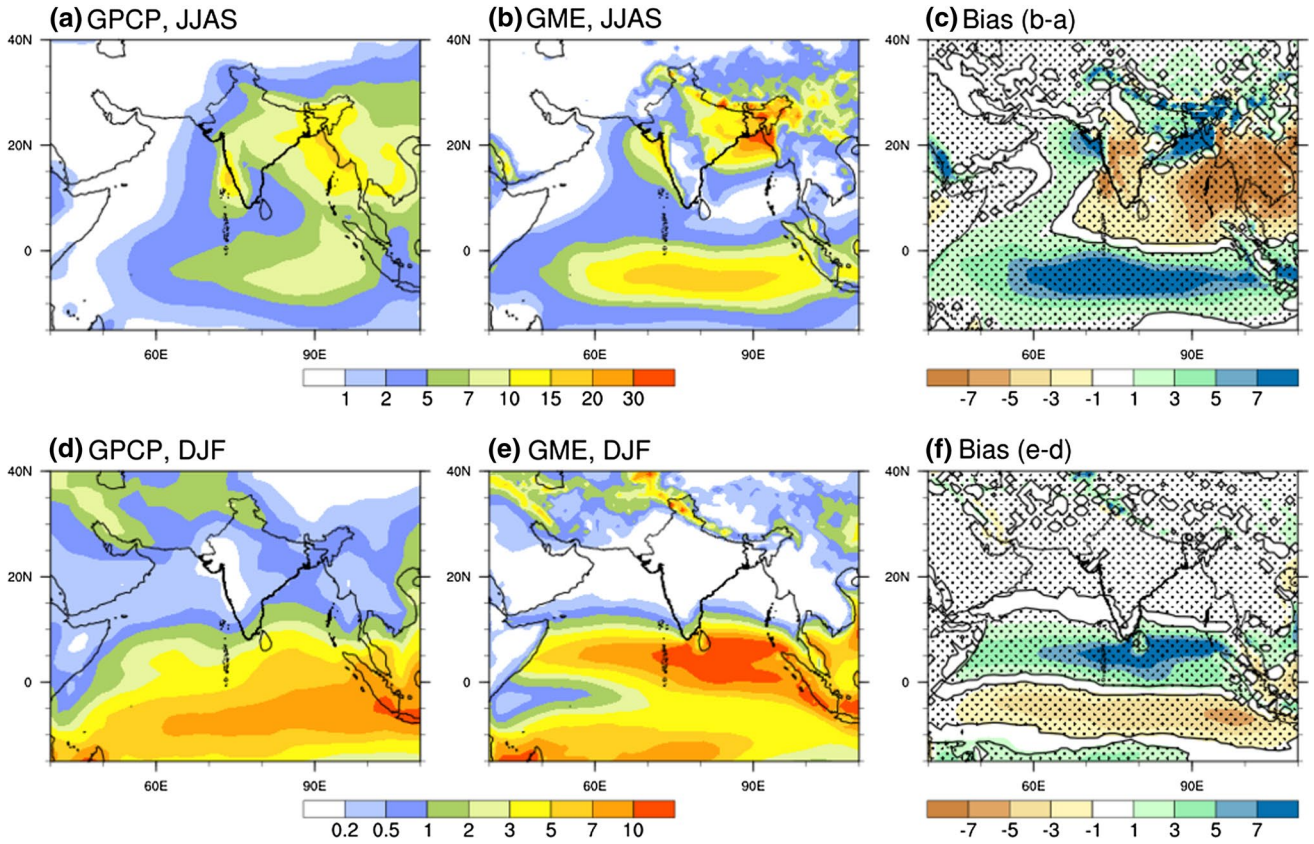

Fig. 1 Climatological seasonal mean precipitation (mm/day) during 1979–2008 (30 years) in **a**–**c** JJAS (June–September) and **d**–**f** DJF (December–February) over South Asian monsoon region in **a** and **d** GPCP observation, **b** and **e** GME and **c** and **f** seasonal biases in GME. The dotted patterns present the level of significance at 95%

precipitation over north and northeast regions (Fig. 1d, e) in DJF. Figure 1c, f illustrates the precipitation biases in GME and GPCP during JJAS and DJF seasons. Compared to the GPCP, the model depicted high positive biases (Fig. 1c) of 5–7 mm/day over large parts of the oceanic regions and extreme northeast India in JJAS. GME-simulated precipitation has a positive bias of 1–5 mm/day over NCI (central northeast India) and negative biases over west Ghat (5–7 mm/day). While large portions of peninsular India have shown negative biases of less than 3 mm/day. Similar biases of high and low precipitation zones are also mentioned in Preethi et al. (2017a, b) using CMIP5 model. During DJF (Fig. 1f), positive biases can be seen above the equator and negative biases below the equator over the Indian Ocean. While over Indian landmass, GME well-captured (large white portions) the precipitation patterns. To examine whether the biases are significant, we have applied the statistical significant tests on the biases (Fig. 1c, f). The biases at 95% significant level are shown by black dots. Large biases are noticed over oceanic sectors, while low biases can be seen over landmasses.

Seasonal precipitation and biases in GME simulation against the IMD data set during JJAS and DJF seasons over the Indian landmasses are also analyzed and are shown in Fig. 2a–f. Compared to the IMD, GME has shown the positive and negative biases over large parts of India and they are similar to those in Fig. 1. However, major differences can be seen over the peninsular India, where GME-simulated precipitation has negative biases of up to 1–3 mm/day over large parts of peninsular India. Over northeast and north-central India, GME has positive biases of up 1–5 mm/day in JJAS. While in DJF (Fig. 2d, e), GME simulation has shown a very low bias over Jammu and Kashmir, north India, and northeast India. Here also, similar nature of biases is noticed, as shown in Fig. 1c, f. It is interesting to note that GME has shown less biases with IMD compared to GPCP over Indian land masses especially in JJAS. It is also appears that GME behaves

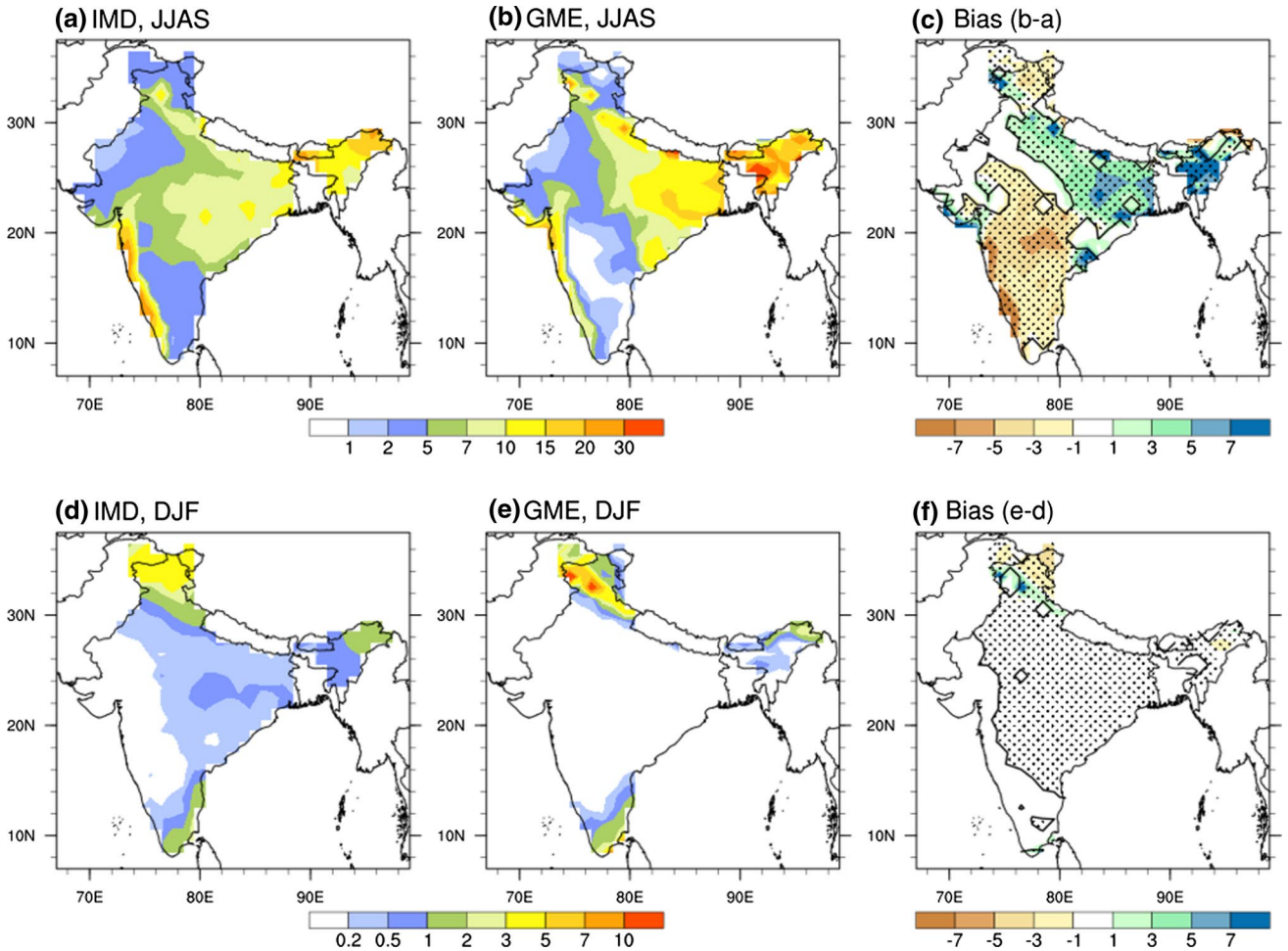

Fig. 2 Climatological seasonal mean precipitation (mm/day) during 1979–2008 (30 years) in **a**–**c** JJAS (June–September) and **d**–**f** DJF (December–February) over Indian landmass in **a** and **d** IMD observation, **b** and **e** GME and **c** and **f** seasonal biases in GME. The dotted patterns present the level of significance at 95%

differently over different parts of the Indian land mass. This suggests that the model-simulated biases in seasonal precipitation could be attributed to errors in simulating the exact locations of precipitation maxima, as reported in several other global models also (Annamalai et al. 2007).

Figure 3a–c presents the variations in JJAS mean precipitation in the first (1979–1988) and last (1999–2008) decades for IMD, GPCP, and GME. Analysis indicates that the GME (Fig. 3c) well-captured the observed characteristics of IMD (Fig. 3a) with an increasing precipitation bands in the foothills of Himalaya and over east coast of India. Over northeast India, IMD and GPCP have shown a decreased precipitation of 2–5 mm/day compared to the GME (1–2 mm/day). While over the west coast, GPCP has shown the largest decrease in precipitation of 5 mm/day compared to the GME and IMD. It is interesting to note that over Indian landmass, high precipitation spreads over large parts of India in IMD and GME (large green and blue patches) compared to the GPCP. The maximum increase in JJAS precipitation can be seen in IMD and GME in the range of 1–5 mm/day and only 1–2 mm/day in GPCP (Fig. 3). While a maximum decrease in precipitation was 5 mm/day (northeast) in IMD and GPCP (west coast), but less than 2 mm/day (northeast and west coast) can be noted in GME. Results of the above analysis indicate that the GME closely captured the important features of observed patterns of seasonal rain in the present-day climate simulation compared to GPCP. The purpose of the initial and last decade's analyses is to assess whether GME reproduces the characteristics of seasonal precipitation within the present-day climate period. This analysis definitely enhances the belief and confirms the use of GME for the study of future climate characteristics. Overestimated precipitation in GME can be investigated by examining the wind fields.

3.2 Wind analysis

The present section compares the performance of GME in simulating the mean JJAS wind fields with NCEP2 (observed) at lower (850 hPa) and upper (200 hPa) levels. The main features of the winds during JJAS are westerlies at lower and easterlies at upper levels. Another important feature of the wind at the lower level is low-level jet over the Arabia Sea and a huge anticyclone (called Tibetan anticyclone) at the upper level. Figures 4a, c and 5a, c display the observed (NCEP2) and model (GME)-simulated JJAS wind fields, and Figs. 4b, d and 5b, d show the difference wind fields between the initial and last decades during 1979–2008 at 850 and 200 hPa, respectively. Results indicate that the GME well-reproduced the mean position of the low-level jet at 850 hPa and upper level Tibetan anticyclone and easterly jet (EJ) over the latitude of southern parts of India at 200 hPa. The wind at 850 hPa is underestimated over the Arabian Sea, but GME realistically reproduced the cross-equatorial flow from southern to northern hemisphere and southeasterly trade winds in the lower troposphere (Fig. 4c). The GME satisfactorily simulated the weaker monsoon westerlies over the Arabian Sea during last decade of the present-day climate (Fig. 4b, d). However, GME simulates stronger easterlies over the head BoB, which brings moistures from BoB and provides high precipitation over the central northeast and northeast India (as shown in Figs. 1 and 2). Similar results are also noted from the analysis of wind circulation at 200 hPa (Fig. 5a–d). Where GME underestimated the EJ and Tibetan anticyclone in the final decades of the present-day climate simulation, which is noticed in the observations (Fig. 5b, d) also. The present analysis of wind circulations at lower and upper levels appear to be well-represented in GME.

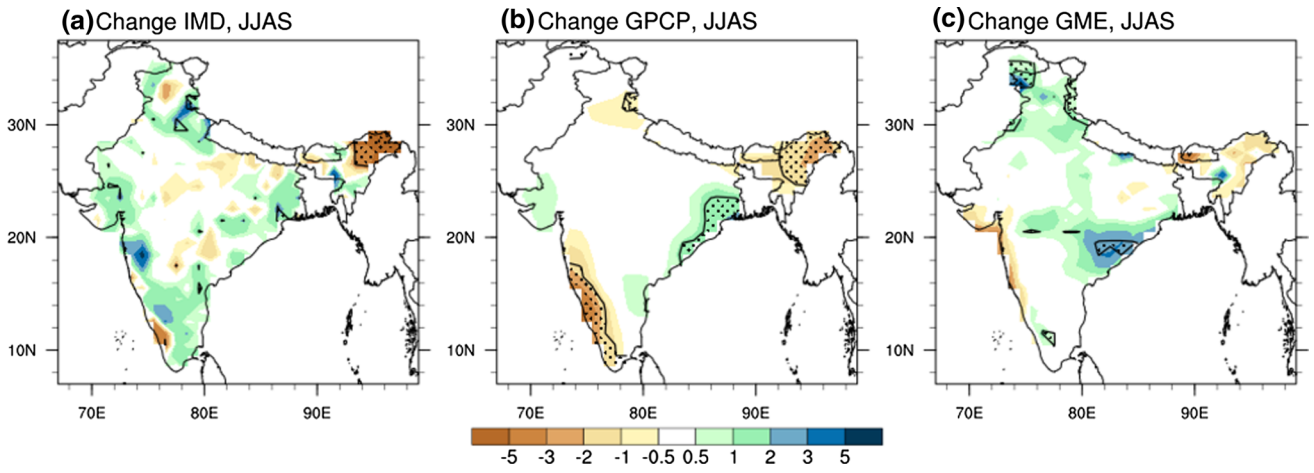

Fig. 3 Changes in mean JJAS precipitation over India between the initial and final decades in the period of 1979–2008 in **a** IMD observation, **b** GPCP observation and **c** GME simulation. The dotted patterns present the level of significance at 95%

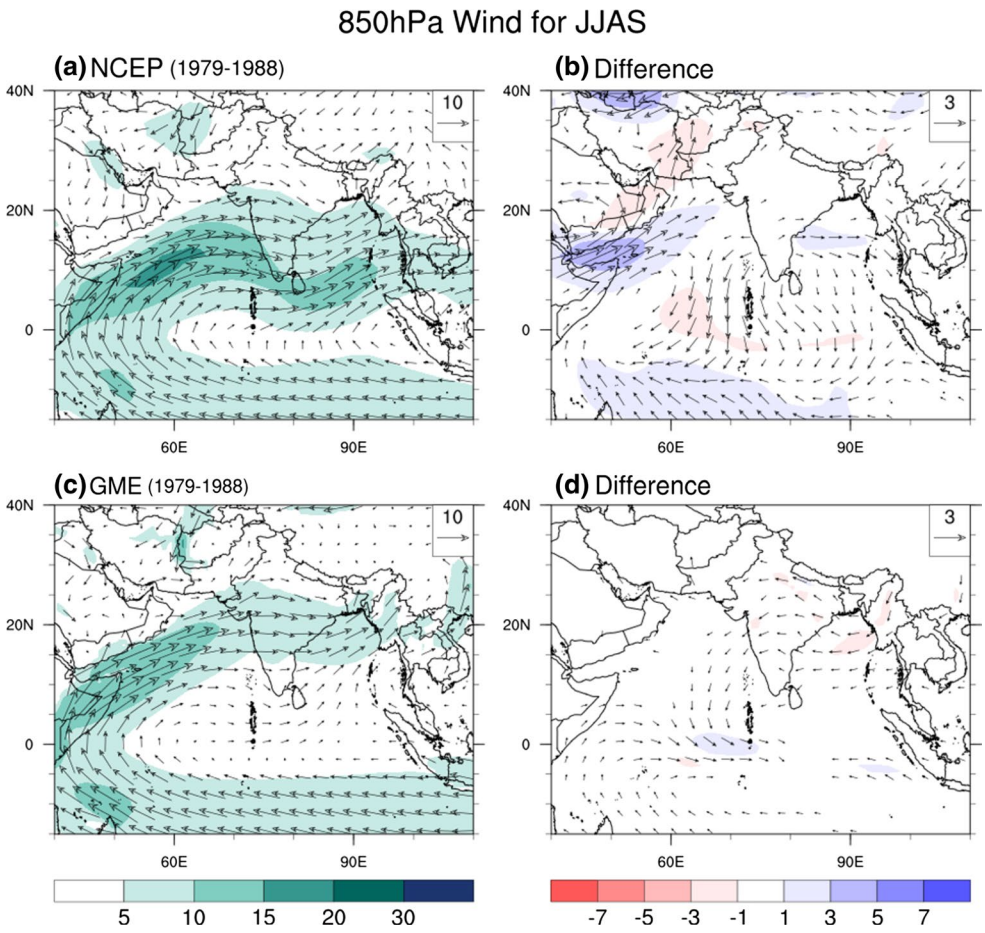

Fig. 4 Mean wind (m/s) fields at 850 hPa in JJAS and their changes between initial and final decades in the period of 1979–2008. The top (**a**, **b**) panel represent the NCEP/NCAR Reanalysis II and bottom (**c**, **d**) panel represent GME simulation, respectively

3.3 Time latitude variations in monthly precipitation

The performance of GME in reproducing the annual cycle of monthly rain over this large domain is investigated to understand how the model performs in different months. Figure 6 shows the annual cycle in zonal-averaged precipitation over the Indian monsoon region (67°–99°E). Here, we have used three observational (GPCP, CMAP, and IMD) data sets for validation of GME performance. Propagation of precipitation over India depicts the distinct northward propagation characteristics of rainband (Fig. 6a–d) that a gradual northward propagation of rainband from south to north is discernible from April to July. The dominant precipitation activity starts from June to September and a retreat after August is noticeable over India. Other noteworthy features are the presence of the Convergence Zone over the equator (not shown here) or zonally aligned zones of precipitation (Sikka and Gadgil 1980) in the southern hemisphere (10°S–Equator). In general, an enhanced (suppressed) precipitation over the oceanic equatorial zone is related to the suppressed (increased) convection over Indian landmass (Sikka and Gadgil 1980). It is to be noted that the northward progression of the oceanic convective zone approaches close to 30°N over the Indian longitude. Compared to other observed data sets, a northward progression of high precipitation band can be seen in IMD and GME also. A high magnitude of northward propagated precipitation of 7 mm/day (yellow contour) can be seen in IMD (above 30°N), GME (close to 30°N), GPCP (close to 28°N), and CMAP (close to 26°N). GME well-captured the northward progression and retreat of monsoon from May to September during summer monsoon season over India (67°–99°E). Although, GME underestimated the seasonal precipitation amount below 20°N (West central region), but well-captured the peaks near 20°N (Western Ghats) and below 30°N (northeast India) when compared to the IMD. While other two observational data due to relatively coarse resolution could not be captured these peak positions clearly. From this validation, it appears that a high-resolution model can be used for the study of monthly and seasonal precipitation over India.

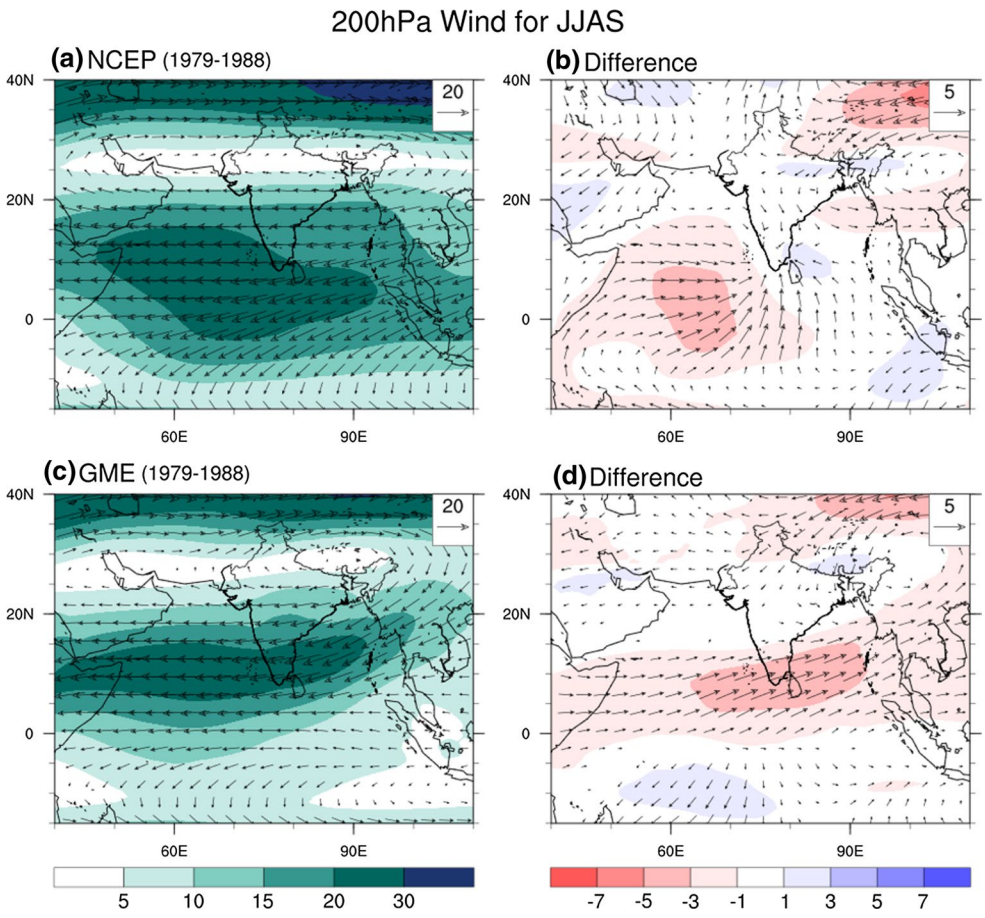

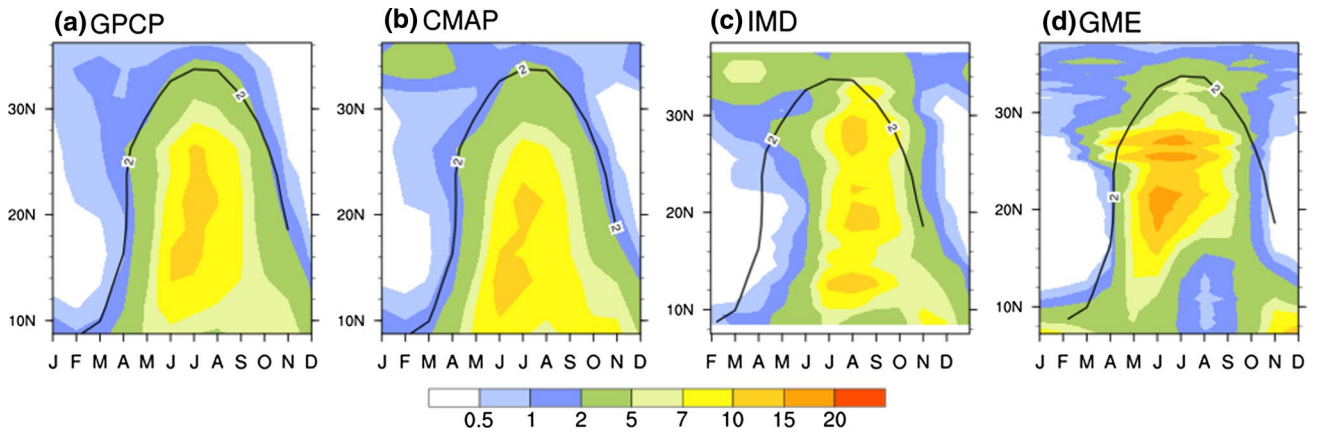

Fig. 5 Same as in Fig. 4 but for the wind at 200 hPa

Fig. 6 Climatological (1979–2008) zonal-averaged monthly mean precipitation (mm/day) **over** Indian (67–99°E) for **a** GPCP, **b** CMAP, **c** IMD, and **d** GME (present day). The black contour line depicts precipitation of 2 mm/day in CMAP observation

These comparative studies of climatological precipitation, circulations, and seasonal migration of precipitation patterns over Indian sub-continent suggest that the GME has abundant reasons for its true use to investigate the changes in the twenty-first century climate over south Asia.

4 Projection of climate and extreme events

4.1 Projected annual temperature and precipitation

Figure 7a, b depicts the GME-projected annual temperature and precipitation relative to the present-day climate

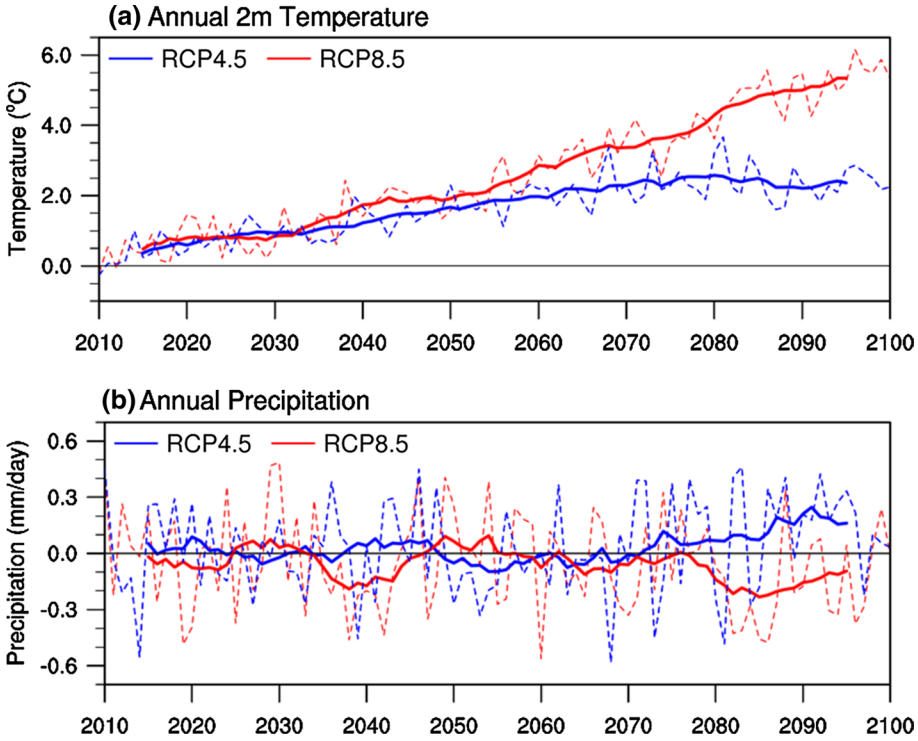

Fig. 7 Interannual (dashed lines) and multidecadal (11-year moving average, solid lines) variations of **a** 2 m temperature anomalies (°C) and **b** precipitation anomalies (mm/day) relative to the present-day climate (1979–2008) during twenty-first century (2010–2100). The blue and red contours represent the RCP4.5 and RCP8.5 scenarios, respectively

(1979–2008) for RCP4.5 and RCP8.5 scenarios over India from 2010 to 2100. Figure 7a shows that the GME (RCP8.5) simulated annual temperature increasing rapidly after 2070 compared to GME (RCP4.5). The year 2096 (6.17 °C) is projected as the warmest year under RCP8.5, while 2081 (3.67 °C) under RCP4.5 during the twenty-first century. Categorizing the number of warm cases (years) having an increase of annual temperature above 2 and 3 °C, analysis identifies 35 cases of above 2 °C and 5 cases of above 3 °C under RCP4.5, with RCP8.5, analysis found 52 cases of above 2 °C, 37 cases of above 3 °C, 23 cases of above 4 °C, 13 cases of above 5 °C, and only one case of above 6 °C (2096) during the study period. While considering the common cases of warm years within the both scenarios, results noted a list of 33 cases of above 2 °C and only five (2068, 2073, 2080, 2081, and 2084 cases) of above 3 °C. It is worth to note that the maximum common warm cases are after 2070. It implies that there is a strong evidence of warming of above 2 °C after 2070 compared to the present-day climate. Considered time slices projections show a warming of 0.7 °C in the end of 2040 s (near-), 1.8 °C in 2070 s (mid-) and 2.4 °C during the end of the twenty-first century (far future) over Indian landmass relative to the present-day climate under RCP4.5. While a warming of 0.8, 2.4, and 4.6 °C is projected with RCP8.5 during the same periods, the regression analysis shows an increasing trend in surface air temperature under both the scenarios, but the rate of increase is higher in a higher scenario.

Figure 7b presents the annual precipitation (mm/day) over Indian landmass from 2010 to 2100 relative to the present-day climate (1979–2008) based on two RCP scenarios. Categorizing the GME-projected flood (based on precipitation $\geq 1\sigma$) and drought (precipitation $\leq -1\sigma$) cases under both the scenarios, the present analysis listed 23 floods and 11 droughts under RCP4.5, while 11 floods and 22 droughts in RCP8.5. Here, regression analysis does not show any trend in precipitation means precipitation. For listing the common years of projected droughts and floods within the both scenarios, the analysis found only three cases in floods and two in droughts. It is interesting to note that 7 floods year out of 23 under RCP4.5 scenario are listed in droughts category under RCP8.5. Here, higher scenario shows higher drought and a lesser flood cases.

4.2 Projected seasonal summer monsoon precipitation

In this section, projected changes in summer monsoon precipitation over India and its surrounding oceanic sectors are studied in detail. As discussed earlier, we have analyzed for the near-, mid-, and far-future time slices and each time slice consists of 30-year period, as mentioned in Figs. 8 and 9, and the period 1979–2008 represents a present-day climate. The possible changes in the future for the twenty-first century are computed by subtracting the present-day climate from the futures. Figures 8a–g and 9a–g present the GME-simulated mean precipitation in JJAS for the present-day and for

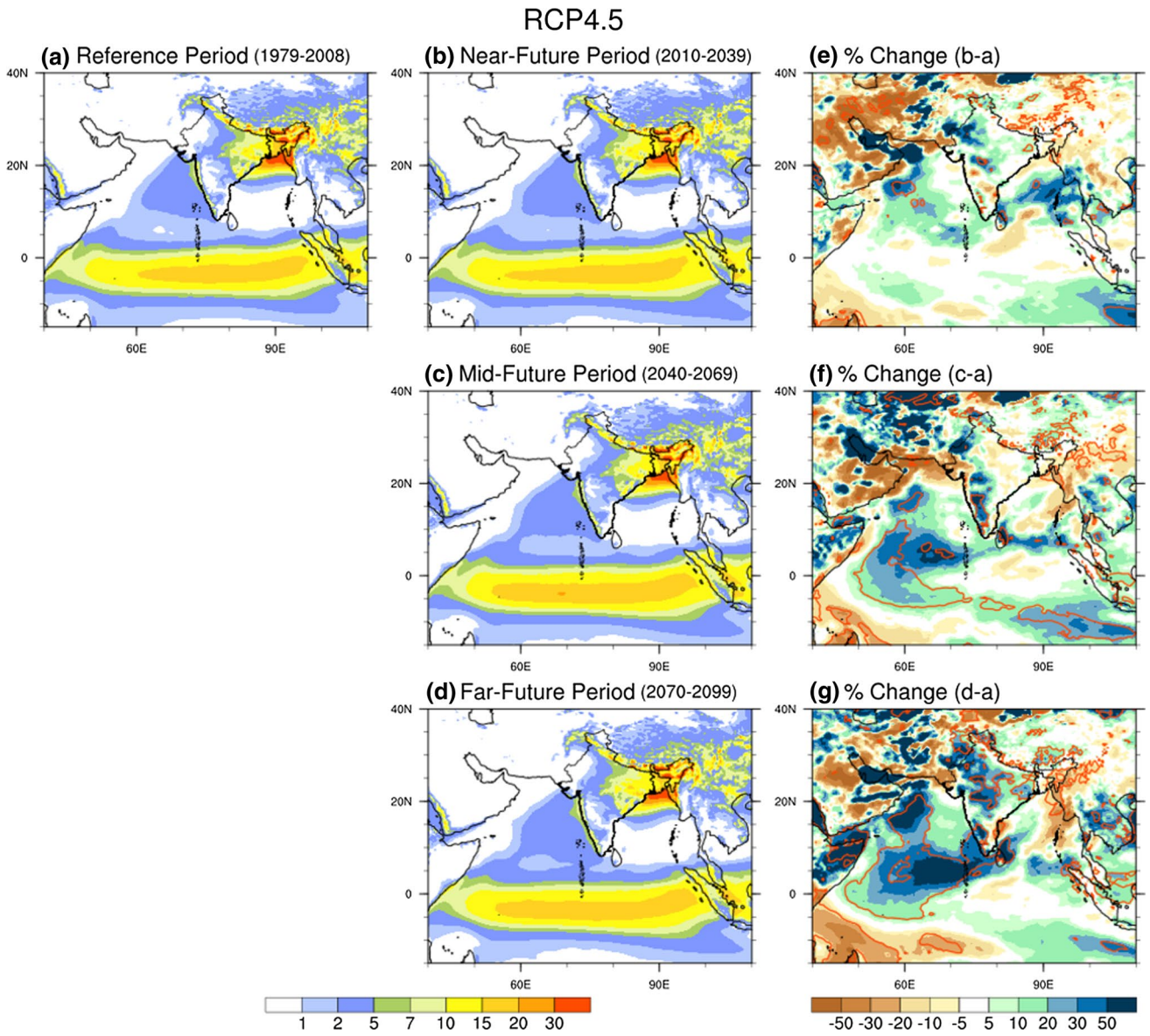

Fig. 8 GME-simulated mean precipitation (mm/day) in JJAS for **a** present day (1979–2008) and projected climates in **b** near- (2010–2039), **c** mid- (2040–2069), and **d** far- (2070–2099) futures under the RCP4.5 scenario and their future changes in percentage during **e** near-, **f** mid-, and **g** far-future climates (right most column). The contours present the level of significance at 95%

three-time slices in the future based on RCP4.5 and RCP8.5 scenarios, respectively. The right columns of Figs. 8 and 9 illustrate the changes during the near-, mid-, and far-future periods. Since India is vast country and JJAS precipitation shows large spatial variations within the same monsoon year. Therefore, it is advisable to emphasize over its different homogeneous regions also to get better regional information. Over Indian landmass, Fig. 8e–g depicts an increase in precipitation over northwest India (NWI), south peninsular India (SPI), and west peninsular India (WPI) in the range of 4–19% from the near- to far futures and a decrease of about 5% in precipitation is noted over the northeast India (NEI) during the same period under RCP4.5. While for RCP8.5, Fig. 9e–g shows an increase of about 5–50% over the SPI and WPI from the near- to far-future periods and a decrease of about 15% over NWI in the near future. This analysis does not support the finding of Dash et al. (2015) using a RegCM4 model and Josepth et al. (2016), and both the studies have reported a reduction in seasonal precipitation over the southern parts of India in mid-century. After all, most of the study has suggested a revival of summer monsoon precipitation activity similar to the GME projection in the far future. Over the Arabian Sea, high successive precipitation is noted from the near- to far-future periods under both

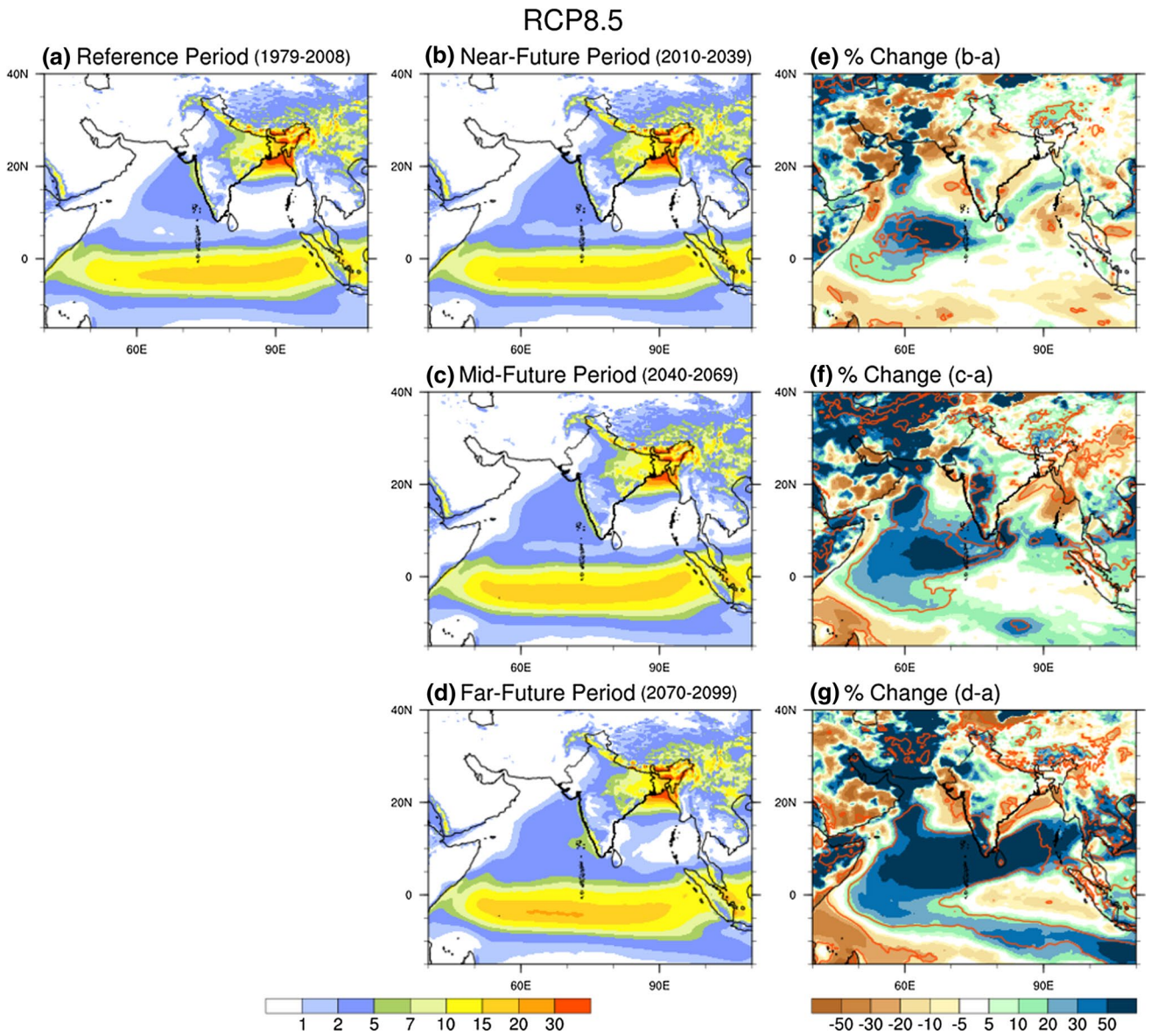

Fig. 9 Same as in Fig. 8, but for the RCP8.5 scenario

the scenarios, but the rate of increase over the Arabian Sea is larger in higher forcing (RCP8.5) compared to the stable (RCP4.5) scenario. Analysis of percentage change in projected JJAS precipitation relative to the present-day climate over Indian landmass shows an increase of about 7.4% in near-, 7.6% in mid-, and about 18% during the far future under RCP4.5. While a little change in near-, but an increase of about 14–18% is projected during the mid-to-far future under RCP8.5.

4.3 Projected seasonal circulations

Some of the past studies found a wind–precipitation paradox over the Asian monsoon sectors while estimating the future precipitation changes. Most of the research papers mentioned an increase in seasonal summer precipitation over India in spite of weak south westerlies and tropical circulations. They have stated that the warming climate enhanced the moisture fluxes towards the continent and it leads to high precipitation (IPCC 2007; Stevenson et al. 2006; Ueda et al. 2006). The other monsoon systems play a key role in increasing/decreasing the seasonal precipitation, are monsoon trough, Mascarene High, and Tibetan High, and are also investigated in the present study.

The projected change in wind fields at 850 hPa for the above-mentioned scenarios during the near-, mid-, and far-future climates is illustrated in Figs. 10a–g and 11a–g, respectively. The wind patterns show anomalous

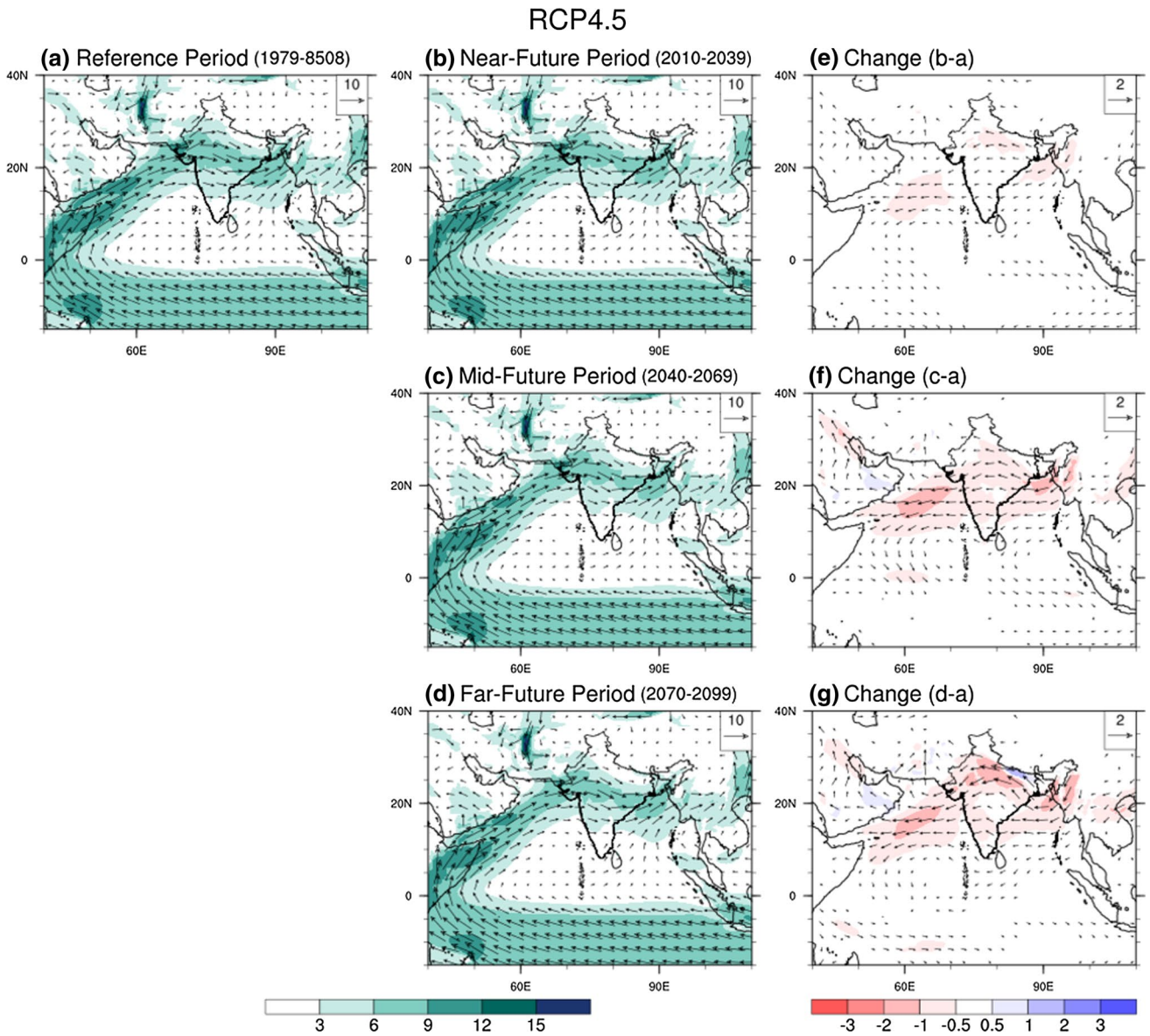

Fig. 10 GME-simulated mean wind (m/s) field at 850 hPa in JJAS for **a** present-day (1979–2008) climate and projected in **b** near- (2010–2039), **c** mid- (2040–2069), and **d** far- (2070–2099) futures under the RCP4.5 scenario and their corresponding changes (in m/s) in **e** near-, **f** mid-, and **g** far-future periods

northeasterly/easterly flows and are dominant over large parts of India indicating a weakening of westerlies in both the emission scenarios. A similar weakening in wind component (precipitation–wind paradox) can be seen in Ueda et al. (2006) under different scenarios simulations. Compared to RCP4.5, the RCP8.5 scenarios have shown stronger northeasterly/easterly flows over the study domain from the mid- to far-future periods. However, there is an indication of southerly/southwesterly winds over the Arabian Sea and a part of Pakistan close to 20°N, and west of 60°E indicated some shifting in the monsoonal flow. A similar weakening of circulation systems is also mentioned in most of the IPCC AR4 models under different global warming experiments and this weakening could be associated with hydrological cycle (Vecchi and Soden 2007; Held and Soden; 2006). In mid-period under both scenarios, the changes in circulations are significant mostly in Northern Hemisphere. While for the far future, there is an indication of weak circulation in Southern Hemisphere. This weak circulation during different time slices suggests that the cross-equatorial flow declines itself in strength due to global warming. A similar weakening in monsoon circulations is also suggested in Tanaka et al. (2005) during the far-future climate. The model projected anomalous northeasterly flow over BoB carrying a

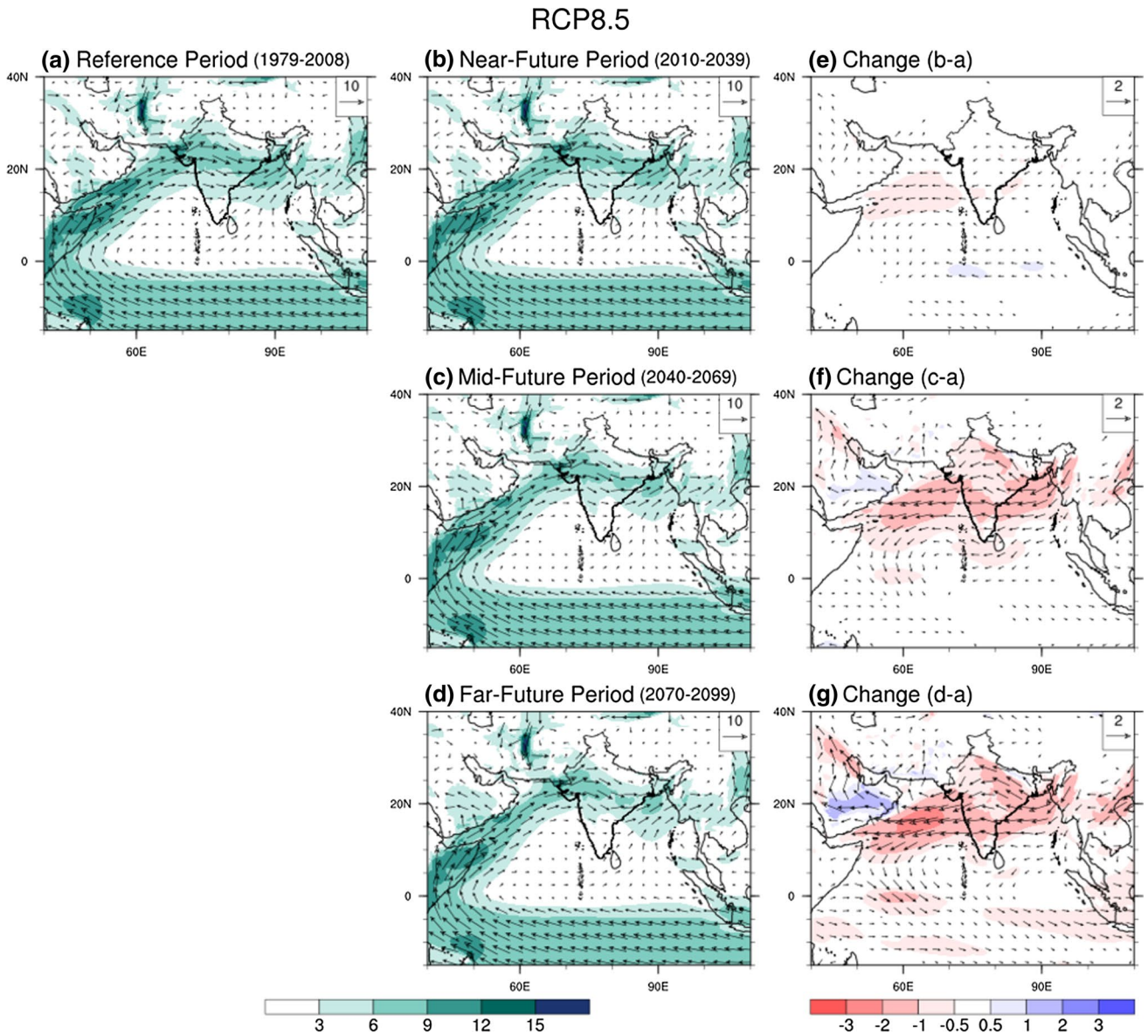

Fig. 11 Same as in Fig. 10, but for the RCP8.5 scenario

moisture fluxes over the Indian sub-continent and it can be attributed with the projected high precipitation over India (as found in Sect. 4.2). It is also to be noted that over head Bay of Bengal, there is an indication of anomalous anti-cyclonic circulation from the mid- to far-future periods in both the scenarios, which prevents the evaluation and growth of westward moving low-pressure systems during monsoon season, supports Singh et al. (2014), who has mentioned a significant decline in the frequency of cyclonic disturbances during recent periods.

4.4 Projected components of monsoon circulation system

In the present section, we will investigate the changes in various components of summer monsoon systems, namely, Monsoon Trough (MT), the Mascarene High (MH), and upper tropospheric Tibetan High (TH) in the near-, mid-, and far-future periods relative to the present-day climate condition using GME model. The MT is an elongated zone of a low-pressure system which extends from northwest India to head BoB during the northward progress of summer monsoon. The MT oscillates in north and south directions from the climatological normal. When it is shifted close to the foothills of Himalayas, a break monsoon conditions is

noticed over large parts of India. The position of MT is generally represented by the mean sea-level pressure.

Figure 12a, b depicts the GME-projected climatological position of the south Asian MT under two different emission scenarios (RCP4.5 and RCP8.5) in the present-day (reference), near-, mid-, and far-future periods. An eastward extension of the eastern edge of the MT into BoB is generally considered as a favorable condition for good monsoon activities over South Asia. The used model, in general, has projected the patterns (intensity) similar to the present-day climate under both the scenarios. The western edge of the trough is located around 67.5°E and eastern edge is around 87.5°E in the present-day climate. It is interesting to note that the GME-projected elongated zone of low-pressure area is be noticed in west close to the northwest India and Pakistan. There is no any significant shift in west portion of MT while comparing with the present-day climate, but an eastern edge exhibited a westward shift by more than 2° longitudes relative to the present-day climate mainly during the mid-to-far-future periods. This large westward shifting can be considered as a weakening of the MT, and projected low precipitation in JJAS over the northeast and north-central India (as mentioned in Sect. 4.2) during the mid- and far-future periods.

Another prominent component plays an important role for ISMR is Mascarene High (MH). The location of MH can be traced on mean sea-level charts and it is normal position mentioned over the West Indian Ocean close to the Madagascar. It is interesting to note that the strength of MH directly associated with monsoon westerlies and moisture flux over the Indian landmass. Similar to MT, the MH swings north–south and east–west directions from its normal position during JJAS season. Figure 13a, b illustrates the projection of MH using the above-mentioned scenarios in the present-day (black contour), near- (green), mid- (blue), and far- (red) future periods. Figure 13a, b shows an intensification of MH mainly towards the eastern edge compared to the west edge relative to the present-day climate. A more eastward extension can be seen in RCP8.5 as compared to

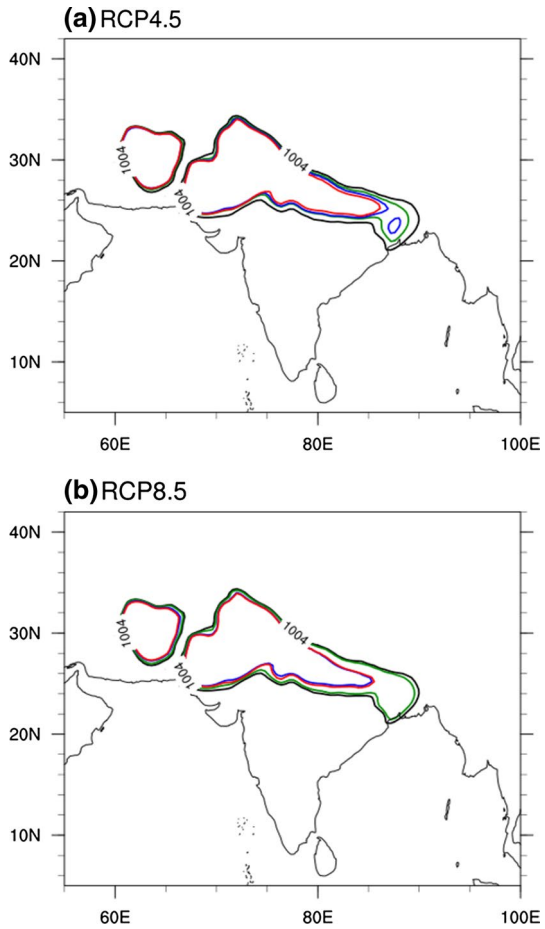

Fig. 12 GME-simulated mean position of South Asian summer monsoon trough in JJAS, represented by closed contours in mean sea-level pressure (hPa), during present day (1979–2008, black contours) and projected future climates in the near- (2010–2039, green contours), mid- (2040–2069, blue contours), and far- (2070–2099, red contours) future using **a** RCP4.5 and **b** RCP8.5 scenarios

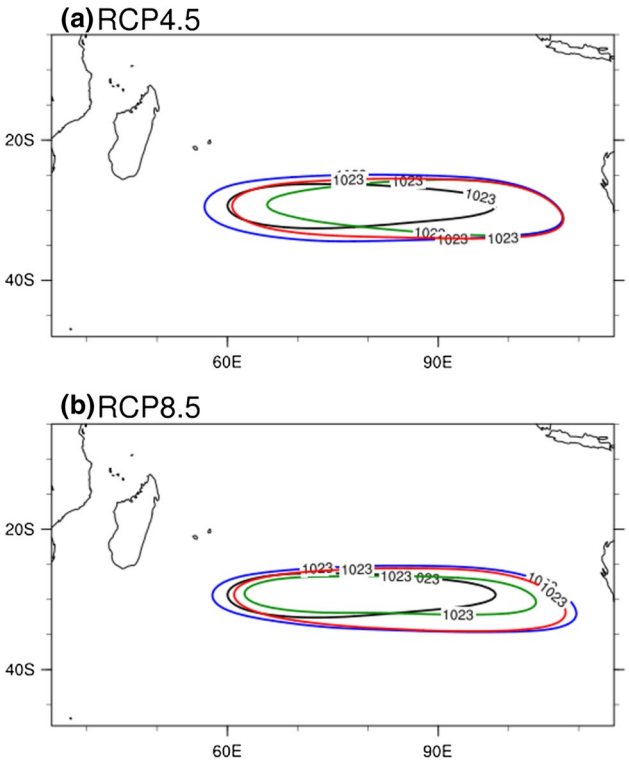

Fig. 13 GME-simulated mean position of Mascarene High (MH) in JJAS, represented as closed contours in mean sea-level pressure (hPa), during present day (1979–2008, black contours) and projected future climates in the near- (2010–2039, green contours), mid- (2040–2069, blue contours) and far- (2070–2099, red contours) future with the **a** RCP4.5 and **b** RCP8.5 scenarios

the RCP4.5 during the study period. A large eastward extension as compared to the westward under both the scenarios can be linked with weak monsoon westerly over the Arabia Sea and a slightly stronger easterly/northeasterly over BoB as noticed in wind analysis (Sect. 4.3) during the near-, mid-, and far-future periods.

Third important component considered in the present study is Tibetan High (TH). The TH plays very important role in enhancing the heat low over India in JJAS and finally ISMR (Wei et al. 2014). It is a high-pressure area at 200 hPa (strong anticyclone) over the Tibet regions. The TH is oriented from east to west directions and generally centered on 88°E. The westerlies are dominant to north of TH and easterlies to south. The spatial distribution of seasonal precipitation is closely connected with the strength and position of TH during the monsoon period.

An intensification and expansion of TH in the present study is depicted by upper tropospheric (200 hPa) geopotential height (Fig. 14). Strengthening of westerlies in the northern flank and weakening of easterlies in the southern flank of TH are associated with the expansion of TH. Figure 14a, b shows an expansion and intensification appears more in west limb rather than its east limb in the near-, mid-, and far-future periods compared to the present-day climate. Southeastward (northwestward) shift of TH is associated with less (high) precipitation over India particularly over NEI and north-central India and this is consistent with the results of Preethi et al. (2017a, b) which is using observation data sets (Preethi et al. 2017a) and based on CMIP5 coupled model projections (Preethi et al. 2017b). Southeastward extension of TH (Fig. 14a, b) can be associated with low precipitation mainly over northeast India (as mentioned in Sect. 4.2). The orientation and strength of TH are very closely associated with the increased sea-surface temperature (SST) over the Indian and west Pacific Oceans (Zhou et al. 2009). Figure 14a, b shows that the western edge of TH is expanding more southeastward rather than northwestward compared to the present-day climate under both the scenarios during the twenty-first century can be attributed with high precipitation over large parts of India.

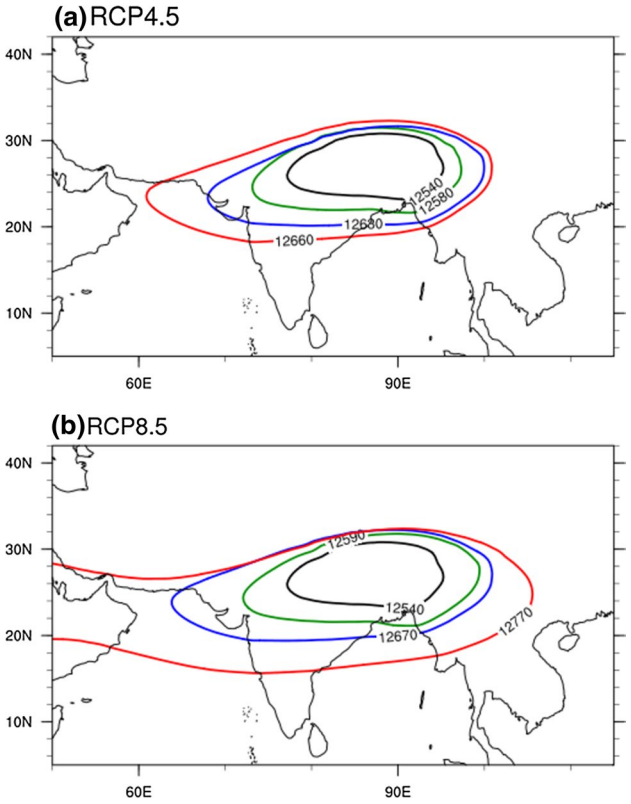

Fig. 14 GME-simulated mean position of South Asian High in JJAS, represented as closed contours in geopotential height (m) at 200 hPa, during present day (1979–2008, black contours) and projected future climates in the near- (2010–2039, green contours), mid- (2040–2069, blue contours) and far- (2070–2099, red contours) future with the **a** RCP4.5 and **b** RCP8.5 scenarios

4.5 Projected seasonal summer monsoon extreme precipitation events

Under the background of global warming, extreme events also changed in frequency and intensity, even more significantly than the mean climate. Meehl et al. (2007) projected an increase in heavy rain events over wide portions of the continent and also seasonal summer precipitation is likely to be increased. They also mentioned that the features of extreme events will be more devastating in nature on regional scales. For Indian sub-continent, a country with a vast territory that is also sensitive to the impact of global warming requires more detail study on extreme precipitation events. An attempt for the projection of extreme precipitation events over India under global warming scenarios is thus more fruitful to elaborate any national climate change mitigation policies.

Here also, a GME model is used to project the changes in the behavior of future summer (JJAS) extreme precipitation intensity in JJAS under the above-mentioned emission scenarios. We have examined the several extreme precipitation indices, as discussed in Klein et al. (2009) and Zhang et al. (2011). The WDAY is defined as the number of rainy days having daily precipitation ≥ 1 mm/day and R20D presents the number of heavy rainy days of ≥ 20 mm/day. We have also studied the longest spells of consecutive dry days (CDD) (daily precipitation < 1 mm/day). Figure 15a–r illustrates the future changes in extreme precipitation indices like WDAY, R20D, and CDD in three-time slices as mentioned above relative to the present-day climate (1979–2008) over India. Analysis of Fig. 15a, b depicts that over northwest India, WDAY increases by 5–20% under RCP4.5 and around 5–10% over south peninsular India in RCP4.5 and RCP8.5

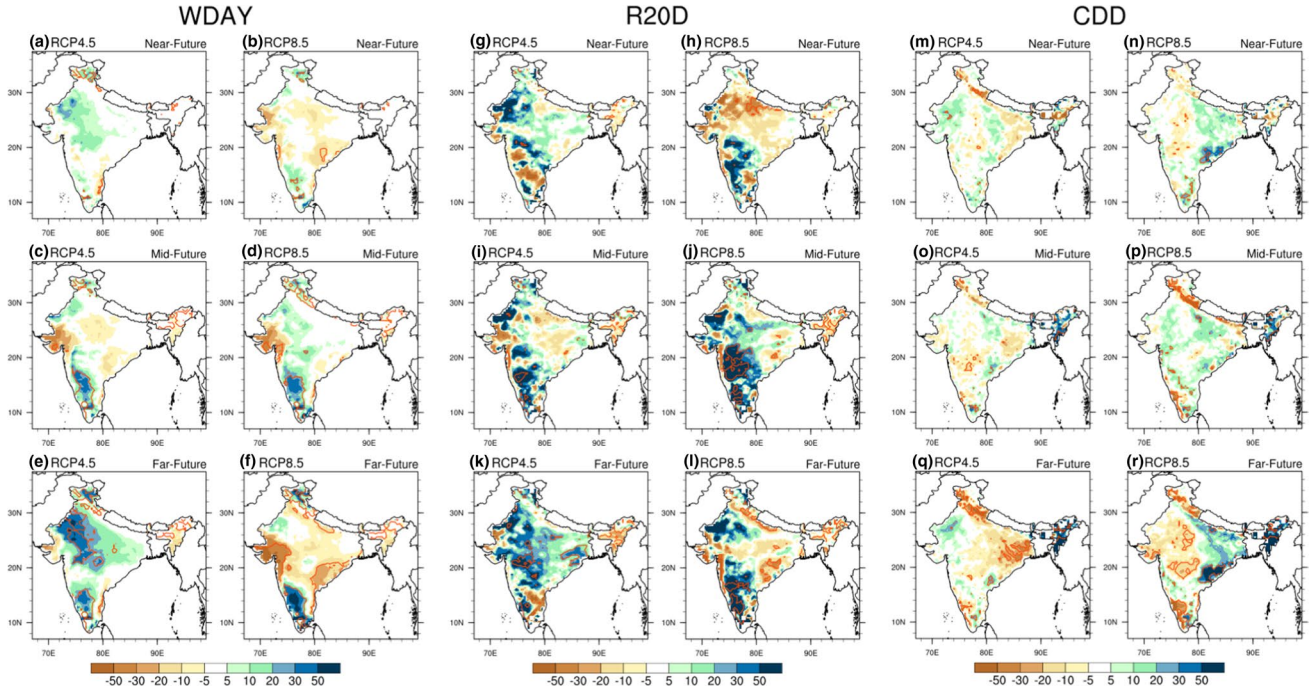

Fig. 15 Assessment of changes (%) in seasonal (JJAS) extreme precipitation indices in **a–f** WDAY (number of days having precipitation ≥1 mm/day), **g–l** R20D (number of days having precipitation ≥20 mm/day) and **m–r** CDD (longest spells of consecutive dry days; precipitation <1 mm/day) for the near- (2010–2039), mid- (2040–2069) and far- (2070–2099) futures relative to the present day (1979–2008) over Indian landmass with the RCP4.5 and RCP8.5 scenarios, respectively. The contours present the level of significance at 95%

in the near future. While during the same period, RCP8.5 projected a decrease of about 5–10% in WDAY over large portions of central India (Fig. 15b). During the mid-to-far-future periods, both the scenarios projected a significant (95% level) increase of about 20–30% in WDAY (Fig. 15c–f) over the west-southern peninsula. Moreover, RCP4.5 projected a significant increase of about 5–10% over large parts of central India during the far future, while a decrease of about 5–50% is projected over large parts of India under RCP8.5 during same period (far future) (Fig. 15f). Both the scenarios have projected a decrease in WDAY over the northeast India during the twenty-first century (Fig. 15e, f).

For the heavy rain events, analysis of Fig. 15g, i, k shows an increase of 5–50% in R20D over northern parts of India in the near future, small portion of northwest India and over a wide area of peninsular India in mid- and a gradual intensification and spread over larger portions during the far future with RCP4.5. While for RCP8.5, Fig. 15h, j, l shows a reduction in R20D over large portions of north India and an increase of 10–50% over peninsular India in the near future. The R20D intensifies and widens from the mid- to far future over the northwest and south peninsular India. Here also, GME projects a reduction in R20D over larger parts of northeast India and an enhancement over the peninsula and northwest India with both the scenarios.

In the case of CDD (Fig. 15m–r), it shows a reverse pattern especially over northwest and north-central India under both scenarios. RCP4.5 projects an enhancement of 5–10% in CDD over northwest India and a reduction over large parts of the central northeast India, while RCP8.5 projects a reverse pattern; an increase in the central northeast and a decrease over northwest India in the near-future climate. While for the mid future, the patterns are nearly similar as in the near future with RCP4.5, but major differences are noted in RCP8.5 which covers a larger area of CDD compared to RCP4.5 over Indian landmass. Again, during the far-future period (Fig. 15q, r), both the scenarios projected an intensification in CDD, a reverse pattern as in the near future. RCP4.5 have shown a decrease in CDD over north-central India and an increase over northwest India, while RCP8.5 projects an increase in CDD over north-central India and a decrease over northwest India. Here also, over northeast India, there is an increase in CDD over larger portions in the near future which is gradually intensifying up to more than 30% and spreads over larger areas in the far future with both the scenarios. A comparison of CDD spells under both the scenarios depicts that the CDD is largely increasing with RCP8.5 as compared to the RCP4.5 over large parts of the Indian landmass. A large number of drought cases projected under RCP8.5 (see Sect. 4.1) may be attributed to the high

CDD events over large parts of India as compared to the RCP4.5.

Overall, analysis of seasonal extreme rain events supports the outcome of Kumar et al. (2006) and Krishnamurthy et al. (2009) who have mentioned a significant increase in heavy rain events over large parts of northwest and southwest regions and a decrease in central northeast India. The outcome of the present research is in tune with the other model's projection (i.e., an increase in heavy rain events and a reduction in weak events) in warming climates over India (Meehl et al. 2000; Semenov and Bengtsson 2002).

5 Summary and conclusions

The present paper uses a high-resolution atmospheric General Circulation Model (GME) for the study of future climate change over India during the twenty-first century. For this long-term climate simulation, we have performed the present-day climate simulation at a 40-km horizontal resolution for 30 years (1979–2008) using AMIP observation. For future climate projection, GME is integrated from 1979 to 2009 for the present-day climate and subsequently the future climate simulation from 2010 to 2100 with RCP4.5 and RCP8.5 scenarios. Before the analysis of future climate projection over India, GME reliability was evaluated by simulating the seasonal monsoon precipitation and annual cycle and it is validated against three observation precipitation (CMAP, GPCP, and IMD) data sets and seasonal circulations against the NCEP2. Validation shows that the GME captures the seasonal precipitation pattern satisfactorily over India with a reliable pattern correlation of above 0.9. The occurrence of high precipitation over the west coast of India, the head of BoB, and its extension towards the south of the equator are also well-reproduced. The analysis of the present-day climate shows that the GME captured the major precipitation characteristics like high precipitation belts over northeast and west coast of India and low precipitation over northwest and east coast of India. GME also well-captured the annual cycle, onset, and withdrawal of seasonal precipitation validated against the various observed data sets.

The future projections of precipitation with both the scenarios have shown a systematic increase over wider portions of India from the near- to far future. This consists of strengthening of summer precipitation over northwest India, south peninsular India (5–50%), and weakening of monsoon over the northeast India and Gujarat (20–30%) regions compared to the present-day climate condition. Projected large-scale circulation features associated with the seasonal precipitation depict a westward shift especially in MT over south Asia by 2°–3° longitude and the associated large-scale response of MH and an expansion of upper tropospheric TH are also evident. These changes in large-scale circulations modulate the southwesterly flow over the south Asia and precipitation variations are well-matched with the changes in large-scale circulation systems. The analysis of projected heavy rain events (R20D) with both the scenarios has shown an increase of about 10–50% over northwest India and west-south peninsular India, while the analysis of CDD (longest spell of dry days) shows a reverse pattern within both the scenarios from the near- to far-future climates. Over India, the projected high precipitation is in line with the most of the global model projections (IPCC 2007) and a broad direction of projected extreme events of the present study is also consistent with the other model results, as mentioned in Kumar et al. (2006) and May (2004). Although a high-resolution GME may not able to capture accurately the regional climate details in the present-day climate simulation, but these results may provide important information to estimate regionally detail temperature increase and changes in precipitation pattern over South Asia especially over the Indian regions. These results might be utilized to set up both national and regional adaptation strategies for global warming.

Acknowledgements The authors want to acknowledge the Korea Meteorological Administration research and Development Program under Grant KMIPA 2015-6130. We also want to acknowledge the Global Science experimental Data hub Center (GSDC) Project, Korea Institute of Science and Technology Information (KISTI) for using computing resources.

Appendix 1

Grid generation in GME model

To generate the geodesic grids, a regular icosahedron (Fig. 16) is constructed inside the sphere, such that 2 of its 12 vertices coincide with the North and South Poles. Five of the other 10 vertices are spaced at equal longitudinal intervals of 72° (=360°/5) along a latitude circle at 26.565°N, the other 5 a long a latitude circle at 26.565°S. Connecting nearest neighbors among these 12 points with great circle arcs divides the spherical surface into 20 equal spherical triangles (Fig. 16a). Beginning from this grid, a new finer grid of triangles is generated by connecting mid-points of the spherical triangle sides by an additional set of great circle arcs (Fig. 16b). This process may be repeated until a grid of the desired resolution is obtained (Fig. 16c, d). This

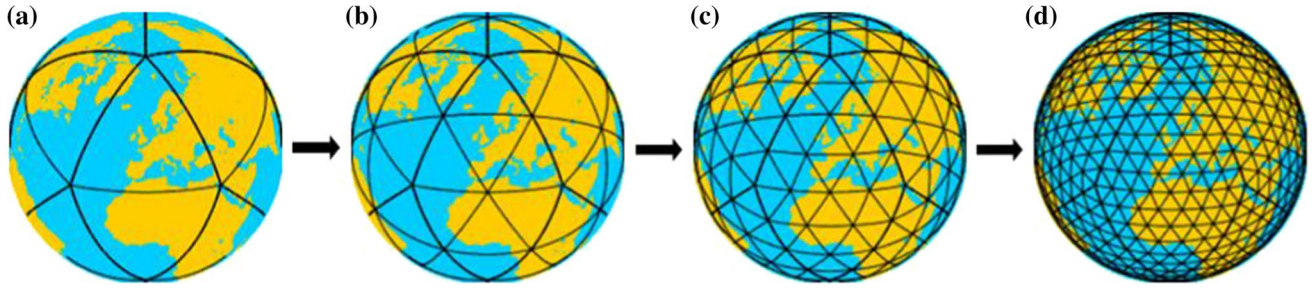

Fig. 16 Geodesic grid generation (Majewski et al. 2002)

Table 2 Some characteristic quantities of the icosahedral–hexagonal grid of GME at different resolutions by n_i, the number of intervals on a main triangle side

n_i	N_{GP}	Δ_{min} (km)	Δ_{avg} (km)	Δ_{max} (km)
16	2562	440.9	477.6	526.4
24	5762	293.9	319.0	347.2
32	10,242	220.4	239.3	263.4
48	23,042	147.0	159.7	173.6
64	40,962	110.2	119.8	131.7
96	92,162	73.5	79.9	86.8
128	163,842	55.1	59.9	65.9
192	368,642	36.7	40.0	43.4
256	655,362	27.6	30.0	32.9
384	1,474,562	18.4	20.0	21.7

$N_{GP}=10n_i^2+2$ is the number of grid points, Δ_{av} is the mean, Δ_{min} is the minimum, and Δ_{max} is the maximum distance between grid points

construction procedure yields a grid consisting of $10n_i^2+2$ grid points (nodes), where n_i is the number of equal intervals into which each side of the original icosahedral triangles is divided. Such grids are quasi-homogeneous in the sense that the area of the largest cell is only a few percent greater than the area of the smallest cell. For example, $n_i=192$ has 40 km resolution with 40 layers and it has 368,642 total number of grid points per layer.

The icosahedral–hexagonal grid provides a nearly uniform coverage of the sphere, even though the hexagonal cells vary somewhat in their exact shape and size (Table 2), especially those close to the pentagons. The pentagons are perfectly regular. To increase the available choice of grid resolution, an initial trisection of the main triangles edges followed by bisections may be performed. Specifications for these grids are shown in Table 2.

References

Adler RF, Huffman GJ, Chang A, Ferraro R, Xie P, Janowiak J, Rudolf B, Schneider U, Curtis S, Bolvin D, Gruber A, Susskind J, Arkin P, Nelkin E (2003) The version 2 global precipitation climatology project (GPCP) monthly precipitation analysis (1979–present). J Hydrometeorol 4:1147–1167

Annamalai H, Hamilton K, Sperber KR (2007) The south Asian summer monsoon and its relationship to ENSO in the IPCC AR4 simulations. J Clim 20:1071–1092

Ashfaq M, Shi Y, Tung W, Trapp RJ, Gao X, Pal JS, Diffenbaugh NS (2009) Suppression of south Asian summer monsoon precipitation in the 21st century. Geophys Res Lett 36:L01704. https://doi.org/10.1029/2008GL036500

Ashrit RG, Douville H, Rupa Kumar K (2003) Response of the Indian monsoon and ENSO-monsoon teleconnection to enhanced greenhouse effect in the CNRM coupled model. J Meteorol Soc Jpn 81:779–803

Chaudhari HS (2006) Predictability and prediction of East Asian Summer monsoon: experiments with GCM, Thesis for the Degree of Doctor of Philosophy, Department of Environmental Atmospheric Science, Pukyong National University, South Korea

Dash SK, Jenamani RK, Kalsi RS, Panda SK (2007) Some evidence of climate change in twentieth-century India. Clim Change 85:299–321

Dash SK, Kulkarni MA, Mohanty UC, Prasad K (2009) Changes in the characteristics of rain events in India. J Geophys Res 114:D10109

Dash SK, Mishra SK, Pattnayak KC, Mamgain A, Mariotti L, Coppola E, Giorgi F, Giuliani G (2015) Projected seasonal mean summer monsoon over India and adjoining regions for the twenty first century. Theor Appl Climatol 122:581–593

Doms G, Schättler U (1999) The non-hydrostatic limited-area model LM (Lokal-Modell) of DWD. Part I: Scientific Documentation. Deutscher Wetterdienst (DWD), Offenbach

Giorgi F, Mearns LO (1999) Introduction to special section: regional climate modeling revisited. J Geophys Res 104:6335–6352

Goswami BN, Venugopal V, Sengupta D, Madhusoodanan MS, Prince KX (2006) Increasing trend of extreme rain events over India in a warming environment. Science 314:1442–1445

Heise E, Schrodin R (2002) Aspects of snow and soil modelling in the operational short range weather prediction models of the German Weather Service. Journal of Computational Technologies, Vol. 7, Special Issue: Proceedings of the International Conference on Modelling, Databases and Information Systems for Atmospheric Science (MODAS), Irkutsk, Russia, June 25–29, 2001, 121–140

Held IM, Soden BJ (2006) Robust responses of the hydrological cycle to global warming. J Clim 19:5686–5699

Hong SY, Kanamitsu M (2014) Dynamical downscaling: fundamental issues from an NWP point of view and recommendations. Asia Pac J Atmos Sci 50:83–104

Huffman GJ, Adler RF, Bolvin DT, Gu G (2009) Improving the global precipitation record: GPCP Version 2.1. Geophys Res Lett 36:L17808. https://doi.org/10.1029/2009GL040000

Hurrell JW, Hack JJ, Shea D, Caron JM, Rosinski J (2008) A new sea surface temperature and sea ice boundary dataset for the community atmosphere model. J Clim 21:5145–5153

IPCC (2007) Climate change 2007: the physical science basis. In: Solomon S, Qin D, Manning M, Chen Z, Marquis M, Averyt KB, Tignor M, Miller HL (eds) Contribution of Working Group 1 to the fourth assessment report of the intergovernmental panel on climate change. Cambridge University Press, Cambridge

IPCC (2013) Climate change 2013: the physical science basis. In: Contribution of Working Group 1 to the fifth assessment report of the intergovernmental panel on climate change. Cambridge University Press, Cambridge

Josepth PV, Bindu G, Preethi B (2016) Impact of upper tropospheric cooling trend over central Asia on the Indian summer monsoon rainfall and the Bay of Bengal cyclone tracks. Curr Sci 110:2105–2113

Kanamitsu M, Ebisuzaki W, Woollen J, Yang SK, Hnilo JJ, Fiorino M, Potter GL (2002) NCEP-DOE AMIP-II reanalysis (R-2). Bull Am Meteorol Soc 93:1631–1643

Klein TA, Zwiers F, Zhang X (2009) Guidelines on analysis of extremes in a changing climate in support of informed decisions for adaptation. Clim Data Monit **WCDMP-No. 72, WMO-TD N.1500: 56**

Kripalani RH, Oh JH, Chaudhari HS (2007a) Response of the East Asian summer monsoon to doubled atmospheric CO_2: coupled climate model simulations and projections under IPCC AR4. Theor Appl Climatol 87:1–28

Kripalani RH, Oh JH, Kulkarni A, Sabade SS, Chaudhari HS (2007b) South Asian summer monsoon precipitation variability: coupled climate model simulations and projections under IPCC AR4. Theor Appl Climatol 90:133–159

Krishnamurthy CKB, Lall U, Kwon HH (2009) Changing frequency and intensity of rainfall extremes over India from 1951 to 2003. J Clim 22:4737–4746

Kumar KR, Sahai AK, Kumar KK, Patwardhan SK, Mishra PK, Revadekar JV, Kamala K, Pant GB (2006) High-resolution climate change scenarios for India for the 21st century. Curr Sci 90:334–345

Lee JW, Hong SY (2014) Potential for added value to downscaled climate extremes over Korea by increased resolution of a regional climate model. Theor Appl Climatol 117:667–677

Lott F, Miller M (1997) A new sub-grid scale orographic drag parameterization: its formulation and testing. Q J R Meteorol Soc 123:101–128

Majewski D, Liermann D, Prohl P, Ritter B, Buchhold M, Hanisch T, Paul G, Wergen W, Baumgardner J (2002) The operational global Icosahedral–Hexagonal gridpoint model GME: description and high-resolution tests. Mon Weather Rev 130:319–338

May W (2004) Potential of future changes in the Indian summer monsoon due to greenhouse warming: analysis of mechanisms in a global time-slice experiment. Clim Dyn 22:389–414

Meehl GA, Karl T, Easterling DR, Changnon S, Pielke R Jr, Changnon D, Evans J, Groisman PY, Knutson TR, Kunkel KE, Mearns LO, Parmesan C, Pulwarty R, Root T, Sylves RT, Whetton P, Zwiersl F (2000) An introduction to trends in extreme weather and climate events: observations, socioeconomic impacts, terrestrial ecological impacts, and model projections. Bull Am Meteorol Soc 81:413–416

Meehl GA, Stocker T, Collins W, Friedlingstein P, Gaye A, Gregory J, Kitoh A, Knutti R, Murphy J, Noda A, Raper S, Watterson I, Weaver A, Zhao ZC (2007) Global climate projections, chapter 10. In: Solomon S, Qin D, Manning M, Chen Z, Marquis M, Averyt KB, Tignor M, Miller HL (eds) Climate Change 2007: the physical science basis. Contribution of Working Group I to the fourth assessment report of the intergovernmental panel on climate change. Cambridge University Press, Cambridge, pp 747–846

Müller E (1981) Turbulent flux parameterization in a regional-scale model. ECMWF Workshop on planetary boundary layer parameterization, pp 193–220

Preethi B, Mujumdar M, Kripalani RH, Amita P, Krishnan R (2017a) Recents trends and teleconnections among South and East Asian summer monsoon in a warming environment. Clim Dyn 48:2489–2505

Preethi B, Mujumdar M, Prabhu A, Kripalani RH (2017b) Variability and tele-connections of South and East Asia summer monsoons in present and future projections of CMIP5 Climate models. Asia Pac J Atmos Sci 53:305–325. https://doi.org/10.1007/s13143-017-0034-3

Rajeevan M, Bhate J, Kale KD, Lal B (2006) High resolution daily gridded rainfall data for the Indian region: analysis of break and active monsoon spells. Curr Sci 91:296–306

Rajendran K, Kitoh A (2008) Indian summer monsoon in future climate projection by a super high-resolution global model. Curr Sci 95:1560–1569

Rajendran K, Sajani S, Jayasankar CB, Kitoh A (2013) How dependent is climate change projection of Indian summer monsoon rainfall and extreme events on model resolution? Curr Sci 104:1409–1418

Ramanathan V, Chung C, Kim D, Bettge T, Buja L, Kiehl JT, Washington WM, Fu Q, Sikka DR, Wild M (2005) Atmospheric brown clouds: impacts on South Asian climate and hydrological cycle. Proc Natl Acad Sci 102:5326–5333. https://doi.org/10.1073/pnas.0500656102

Ramesh KV, Goswami P (2007) Reduction in temporal and spatial extent of the Indian summer monsoon. Geophys Res Lett 34:L23704

Ritter B, Geleyn JF (1992) A comprehensive radiation scheme for numerical weather prediction models with potential applications in climate simulations. Mon Weather Rev 120:303–325

Sabade SS, Kulkarni A, Kripalani RH (2011) Projected changes in South Asia summer monsoon by multi-model global warming experiments. Theor Appl Climatol 103:543–565

Saini R, Wang G, Yu M, Kim J (2015) Comparison of RCM and GCM projections of boreal summer precipitation over Africa. J Geophys Res Atmos 120:3679–3699

Scoccimarro E, Gualdi S, Bellucci A, Sanna A, Fogli PG, Manzini E, Vichi M, Oddo P, Navarra A (2011) Effects of tropical cyclones on ocean heat transport in a high resolution coupled general circulation model. J Clim 24:4368–4384

Semenov V, Bengtsson L (2002) Secular trends in daily precipitation characteristics: greenhouse gas simulation with a coupled AOGCM. Clim Dyn 19:123–140

Sikka DR, Gadgil S (1980) On the maximum cloud zone and the ITCZ over Indian longitudes during the southwest monsoon. Mon Weather Rev 108:1840–1853

Singh D, Tsiang M, Rajaratnam B, Diffenbaugh NS (2014) Observed changes in extreme wet and dry spells during the South Asian summer monsoon season. Nat Clim Change 4:456–461

Srivastava AK, Singh GP, Singh OP, Choudhary UK (2015) Recent variability and trends in temperatures over India. Vayumandal 40:161–181

Srivastava AK, Singh GP, Singh OP (2016) Variability and trends in extreme rainfall over India. Mausam 67:745–766

Stevenson DS, Dentener FJ, Schultz MG, Ellingsen K, van Noije TPC, Wild O, Zeng G, Amann M, Atherton CS, Bell N, Bergmann DJ, Bey I, Butler T, Cofala J, Collins WJ, Derwent RG, Doherty RM, Drevet J, Eskes HJ, Fiore AM, Gauss M, Hauglustaine DA, Horowitz LW, Isaksen ISA, Krol MC, Lamarque JF, Lawrence MG, Montanaro V, Müller JF, Pitari G, Prather MJ, Pyle JA, Rast S, Rodriguez JM, Sanderson MG, Savage

NH, Shindell DT, Strahan SE, Sudo K, Szopa S (2006) Multimodel ensemble simulations of present-day and near-future tropospheric ozone. J Geophys Res 111:D08301. https://doi.org/10.1029/2005JD006338

Tanaka HL, Ishizaki N, Nohara D (2005) Intercomparison of the intensities and trends of Hadley, Walker, and Monsoon circulations in the global warming projects. SOLA 1:077–080

Tiedtke M (1989) A comprehensive mass flux scheme for cumulus parameterization in large-scale models. Mon Weather Rev 117:1779–1800

Trenberth KE, Fasullo J, Smith L (2005) Trends and variability in column-integrated water vapor. Clim Dyn 24:741–758

Turner AG, Slingo JM (2009) Uncertainties in future projections of extreme precipitation in the Indian monsoon region. Atmos Sci Lett 10:152–158

Turner AG, Inness PM, Slingo JM (2007) The effect of doubled CO_2 and model basic state biases on the monsoon-ENSO system. I: mean response and interannual variability. Q J R Meteorol Soc 133:1143–1157. https://doi.org/10.1002/qj.82

Ueda H, Iwai A, Kuwako K, Masatake EH (2006) Impact of anthropogenic forcing on the Asian summer monsoon as simulated by eight GCMs. Geophys Res Lett 33:L06703. https://doi.org/10.1029/2005GL025336

Vecchi GA, Soden BJ (2007) Global warming and the weakening of the tropical circulation. J Clim 20:4316–4340

Wei R, Zhang H, Wen M, Rong XY, Li T (2014) Impact of Indian summer monsoon on the South Asian High and its influence on summer rainfall over China. Clim Dyn 43:1257–1269. https://doi.org/10.1007/s00382-013-1938-y

Woo S, Singh GP, Oh J-H, Lee KM (2018) Possible teleconnection between East and South Asian monsoon precipitation in projected future climate change. Meteorol Atmos Phys. https://doi.org/10.1007/s00703-017-05732-2

Xie P, Arkin PA (1997) Global precipitation: a 17-year monthly analysis based on gauge observations, satellite estimates, and numerical model outputs. Bull Am Meteorol Soc 78:2539–2558

Zhang X, Alexander L, Hegerl GC, Jones P, Tank AK, Peterson TC, Trewin B, Zwiers FW (2011) Indices for monitoring changes in extremes based on daily temperature and precipitation data. WIREs Clim Change 2:851–870

Zhao F, Bailey-Kellogg C (1998) Intelligent simulation. AAAI Tutor Forum

Zhou T, Yu R, Zhang J, Drange H, Cassou C, Deser C, Hodson DLR, Sanchez-Gomez E, Li J, Keenlyside N, Xin X, Okumura Y (2009) Why the Western Pacific subtropical high has extended west ward since the late 1970s. J Clim 22:2199–2215